한국소음진동공학회논문집 제 15 권 제 4 호, pp. 437~444, 2005.

Response Characteristics of Aeroelastic Systems Using Robust Controller
강인한 제어기를 이용한 공탄성 시스템의 응답특성

Sungsoo Na and In-Joo Jeong
나 성 수† · 정 인 주*

(Received December 28, 2004 : Accepted March 14, 2005)

Key Words : Aeroelastic Response(공탄성 응답), Uncertainty(불확실성), Multiobjective State-feedback Synthesis(다목적 상태궤환 합성법)

ABSTRACT

This paper presents a robust aeroelastic control methodology of a two dimensional flapped wing system exposed to an incompressible flow field. A robust controller is designed using a linear matrix inequality (LMI) approach for the multiobjective synthesis. The design objectives are to achieve a mix of H_∞ performance and H_2 performance satisfying constraints on the closed loop pole locations in the presence of model uncertainties. Numerical examples are presented to demonstrate the effectiveness of LMI approach in damping out the aeroelastic response of 3-DOF flapped wing system.

요 약

이 논문은 비압축성 유동장에 노출된 2차원 플랩이 있는 날개의 단면에 대한 강인한 공탄성 제어기법을 소개하고 있다. 강인한 제어기는 다목적 상태궤환 합성법을 위해 선형행렬부등식을 이용하여 설계되었다. 제어기의 설계목적은 모델불확실성이 존재하는 상황에서 주파수영역에서의 성능과 시간영역에서의 성능을 함께 만족시키는 것으로 하였다. 수치예제들은 2차원-3자유도 플랩이 있는 날개 단면의 공탄성 응답을 감쇠시키는데 있어서 선형행렬부등식의 접근법의 유효성을 잘 제시하고 있다.

1. Introduction

The next generation of combat aircraft is likely to operate in more severe environmental conditions that in the past. This implies that such an aircraft, in addition to gust, will be exposed, among others, to blast, fuel explosion, and sonic boom pulses.[1,2] Under such conditions, even if the flight speed of the aircraft is below the flutter speed, the wing structure will be subjected to large oscillations that can result in its failure by fatigue. Moreover, in some special events, occurring during the operational life of the aircraft such as escape maneuvers, significant decays of the flutter speed can occur, with dramatic consequences for the further evolution of the aircraft. All these facts fully underline the necessity of the implementation of a robust control capability enabling one to fulfill two basic objectives: a) to enhance the subcritical aeroelastic response, in the sense of suppressing the wing

† Corresponding Author : Members, Korea University, Seoul, Korea
E-mail : nass@korea.ac.kr
Tel : (02) 3290-3370, Fax : (02) 926-9290
*Korea University, Seoul, Korea

oscillations in the shortest possible time even though model uncertainty exists, and b) to extend the flight envelop by suppressing the flutter instability and so, contributing to a significant increase of the allowable flight speed. With this in mind, in this paper the robust aeroelastic control of a 3-DOF flapped wing system exposed to an incompressible flow field will be investigated. In this context, multiobjective state feedback control law implementing mixed H_∞/H_2 control strategy with pole placement constraint will be implemented, and some of its performances will be put into evidence.

2. Configuration of the 3-DOF Flapped Wing Model

Figure 1 presents the typical wing-flap that is considered in the present aeroelastic analysis. The three degrees of freedom associated with the airfoil appear clearly from Fig. 1. The pitching and plunging displacements are restrained by a pair of springs attached to the elastic axis (EA) with spring constants K_α and K_h, respectively. The control flap is located at the trailing edge. A torsional flap spring of constant K_β is also attached at the hinge axis: h denotes the plunge displacement (positive downward), α is the pitch angle measured from the horizontal at the elastic axis of the airfoil (positive nose-up) and β is the flap deflection measured from the control flap hinge (positive flap down).

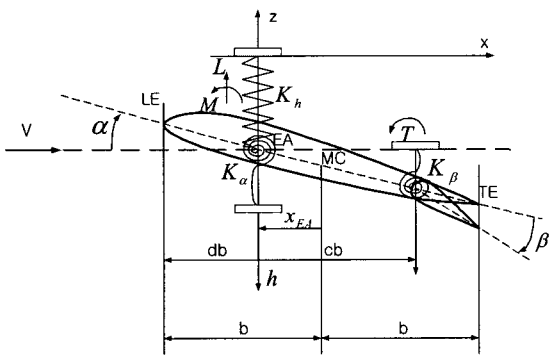

Fig. 1 Typical flapped wing section

3. Governing Equation of the System

In matrix form the aeroelastic governing equations of the 3-DOF flapped wing system can be written as[3,4]:

$$\mathbf{M}\ddot{\mathbf{y}}(t)+\mathbf{K}\mathbf{y}(t)=-\mathbf{L}(t)-\mathbf{L}_g(t)+\mathbf{L}_b(t)+\mathbf{L}_c(t) \quad (1)$$

where $-\mathbf{L}(t)$, $-\mathbf{L}_g(t)$, $\mathbf{L}_b(t)$ and $\mathbf{L}_c(t)$ represent the unsteady aerodynamic, gust, blast and control loads, respectively. In Eq. (1), the column vector of plunging/pitching/flapping displacement is defined as

$$\mathbf{y}(t)=\left[\frac{h(t)}{b} \quad \alpha(t) \quad \beta(t)\right]^T \quad (2)$$

while

$$\mathbf{M}=\begin{bmatrix} bm & S_\alpha & S_\beta \\ bS_\alpha & I_\alpha & I_\beta+bcS_\beta \\ bS_\beta & I_\beta+bcS_\beta & I_\beta \end{bmatrix} \quad (3)$$

$$\mathbf{K}=\begin{bmatrix} bK_h & 0 & 0 \\ 0 & K_\alpha & 0 \\ 0 & 0 & K_\beta \end{bmatrix} \quad (4)$$

denote the mass and stiffness matrices, respectively.

The second order aeroelastic governing equation can be cast in a first order state-space form as:

$$\dot{\mathbf{x}}(t)=\mathbf{A}\mathbf{x}(t)+\mathbf{B}u(t)+\mathbf{G}\mathbf{w}(t) \quad (5)$$

Here $\mathbf{A}$ is the aerodynamic matrix, see Ref. 2. The state vector is given by

$$\mathbf{x}(t)=\left[\dot{h}/b \;\; \dot{\alpha} \;\; \dot{\beta} \;\; h/b \;\; \alpha \;\; \beta \;\; B_1 \;\; B_2 \;\; A_1 \;\; A_2\right]^T \quad (6)$$

where B_1, B_2, A_1 and A_2 denote aerodynamic lag states: $u(t)$ is control input $\mathbf{w}(t)$ is an external disturbance represented by a time-dependent external excitation, such as blast[5], sonic-boom or

step pressure pulse, etc; **G** is the disturbance-input matrix, while **B** is the control input matrix that is given by

$$\mathbf{B}=\frac{1}{I_\beta}\left[\left(\mathbf{M}^{-1}[0\ \ 0\ \ 1]^T\right)^T 0\ \ 0\ \ 0\ \ 0\ \ 0\ \ 0\right]^T \tag{7}$$

The aerodynamic load vector appearing in Eq. (1) is expressed in terms of its components as

$$\mathbf{L}(t)=\left[L(t)\quad M(t)\quad T(t)\right]^T \tag{8}$$

where $L(t)$, $M(t)$ and $T(t)$ denote, respectively, the aerodynamic lift (measurement positive in the upward direction), the pitching moment about the one-quarter chord of the airfoil (positive nose-down) and theflap torque applied to the flap hinge.

The second terms in the Eq. (1) are due to the gust. In this respect, for the gust loading we have[2]

$$\mathbf{L_g}(t)=\left[L_G(t)\ \ M_{yG}(t)\ \ T_{yG}(t)\right]^T \tag{9}$$

where

$$L_G(t)=\frac{1}{2}\rho V^2 b\int_0^t I_{LG}(t-\sigma)\frac{w_G}{V}d\sigma \tag{10}$$

$$M_{yG}(t)=\frac{1}{2}\rho V^2 b^2\int_0^t I_{MG}(t-\sigma)\frac{w_G}{V}d\sigma \tag{11}$$

$$T_{yG}(t)=\frac{1}{2}\rho V^2 b^2\int_0^t I_{TG}(t-\sigma)\frac{w_G}{V}d\sigma \tag{12}$$

herein, w_G is the gust vertical velocity, while I_{LG}, I_{MG} and I_{TG} are the related impulse functions. For the present case of the incompressible flow, we have[2]:

$$I_{LG}=4\pi\psi,\quad I_{MG}=I_{LG}(1/2+x_{EA}/b),\quad I_{TG}=0 \tag{13-15}$$

where ψ is the *Küssner's* function, approximated by [1,2]:

$$\psi(t)=1-0.5e^{-0.13t}-0.5e^{-t} \tag{16}$$

4. Multiobjective State Feedback Control Methodology

In many control problems, the design specifications are based on a mix of performance and robustness objectives expressed both in the time and frequency domains. These various objectives are rarely satisfied with a single synthesis. In this sense, through multiobjective control, we can get a number of control objectives[6]. Multiobjective robust design pertain to the so-called "mixed H_∞/H_2 problem", which corresponds to robust stability and nominal performance for state-feedback and output-feedback cases had been studied in some papers.[7] In summation, multiobjective design allows for more flexible and accurate specification of the desirable closed-loop behavior.

In this paper, multiobjective state-feedback control methodology applied in the wing section is implemented.

4.1 H_∞ Performance

The basic configuration of the state-feedback control structure is shown in Fig. 2. A linear time invariant (LTI) system is described by the state equations as follows[8]

$$\begin{aligned}\dot{\mathbf{x}}(t)&=\mathbf{A}\mathbf{x}(t)+\mathbf{B}_1\mathbf{w}(t)+\mathbf{B}_2\mathbf{u}(t)\\ \mathbf{z}_\infty(t)&=\mathbf{C}_1\mathbf{x}(t)+\mathbf{D}_{11}\mathbf{w}(t)+\mathbf{D}_{12}\mathbf{u}(t)\end{aligned} \tag{17}$$

where $\mathbf{x}(t)$ is the state, $\mathbf{u}(t)$ is the control input,

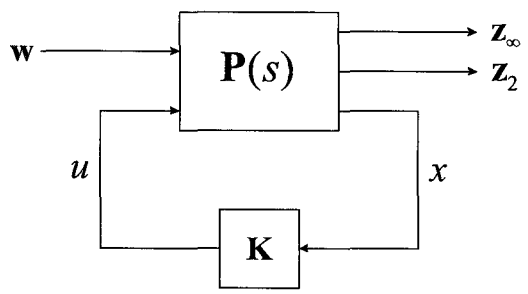

Fig. 2 Standard H_∞/H_2 state-feedback structure

$\mathbf{w}(t)$ is the exogenous input and $\mathbf{z}_\infty(t)$ is the regulated output. The constraint $\|T_{w_\infty}\|_\infty < \gamma$ can be interpreted as a disturbance rejection performance and robust stability of the closed loop system.

By using H_∞ control, a given constant $\gamma > 0$, the system (17) could be stabilizable with disturbance attenuation γ if there exists a state-feedback matrix $\mathbf{K} \in \mathbb{R}^{n_u \times n}$ such that the following LMI conditions are satisfied.

$$\begin{bmatrix} \mathbf{A}\mathbf{Q}_\infty + \mathbf{Q}_\infty\mathbf{A}^T + \mathbf{B}_2\mathbf{L} + \mathbf{L}^T\mathbf{B}_2^T & \mathbf{B}_1 & \mathbf{Q}_\infty\mathbf{C}_\infty^T + \mathbf{L}^T\mathbf{D}_{1u}^T \\ \mathbf{B}_1^T & -\gamma^2\mathbf{I} & \mathbf{D}_{11}^T \\ \mathbf{C}_1\mathbf{Q}_\infty + \mathbf{D}_{12}\mathbf{L} & \mathbf{D}_{11} & -\mathbf{I} \end{bmatrix} \le 0,$$
$$\mathbf{Q}_\infty > 0 \tag{18}$$

where $\mathbf{L} = \mathbf{K}\mathbf{Q}_\infty$.

4.2 H_2 Performance

A state-feedback control system for H_2 control problem is represented as

$$\begin{aligned} \dot{\mathbf{x}}(t) &= \mathbf{A}\mathbf{x}(t) + \mathbf{B}_1\mathbf{w}(t) + \mathbf{B}_2\mathbf{u}(t) \\ \mathbf{z}_2(t) &= \mathbf{C}_2\mathbf{x}(t) + \mathbf{D}_{21}\mathbf{w}(t) + \mathbf{D}_{22}\mathbf{u}(t) \end{aligned} \tag{19}$$

The H_2 state feedback control problem is to find a control gain $\mathbf{K}$ that stabilizes system internally and minimizes the H_2 norm of the transfer matrix T_{wz_2} from $\mathbf{w}$ to $\mathbf{z}_2$. And recall that $\|\mathbf{T}_{wz_2}\|_2^2 = trace(\mathbf{C}_{cl2}\mathbf{Q}_c\mathbf{C}_{cl2}^T)$ where $\mathbf{Q}_c$ is the solution of the Lyapunov equation and controllability Gramian,

$$\|\mathbf{T}_{wz_2}\|_2^2 = trace(\mathbf{C}_{cl2}\mathbf{Q}_c\mathbf{C}_{cl2}^T) < trace(\mathbf{C}_{cl2}\mathbf{Q}_2\mathbf{C}_{cl2}^T)^T < trace(\mathbf{Y})$$

whenever the symmetric matrices $\mathbf{Q}_2$ and $\mathbf{Y}$ satisfy

$$\begin{bmatrix} \mathbf{A}\mathbf{Q}_2 + \mathbf{Q}_2\mathbf{A}^T + \mathbf{B}_2\mathbf{L} + \mathbf{L}^T\mathbf{B}_2^T & \mathbf{B}_1 \\ \mathbf{B}_1^T & -\mathbf{I} \end{bmatrix} < 0,$$

$$\begin{bmatrix} \mathbf{Y} & \mathbf{C}_2\mathbf{Q}_2 + \mathbf{D}_{22}\mathbf{L} \\ \mathbf{Q}_2\mathbf{C}_2^T + \mathbf{L}\mathbf{D}_{22}^T & \mathbf{Q}_2 \end{bmatrix} > 0. \tag{20}$$

where $\mathbf{L} = \mathbf{K}\mathbf{Q}_2$

4.3 Regional Pole Constraints

It is known that the transient response of a linear system is related to the locations of its poles. Pole assignment in convex regions of the left-half plane can also expressed as LMI constraints on the Lyapunov matrix $\mathbf{Q}$. Regions of interest include α-stability regions $\mathrm{Re} \le -\alpha$, vertical strips, disks, conic sector, etc. Another interesting region for control purpose is the set $S(\alpha, r, \theta)$ of complex numbers $x+yj$ such that

$$x < -\alpha < 0, \quad |x + jy| < r, \quad \tan\frac{\theta}{2}x < -|y| \tag{21}$$

as shown in Fig. 3 This is in turn bounds the maximum overshoot, the frequency of oscillatory modes, delay time, rise time and settling time.

$$M_{\Re}(\mathbf{A}, \mathbf{Q}) < 0, \quad \mathbf{Q} > 0 \tag{22}$$

The matrix $\mathbf{A}$ is $\Re$-stable if and only if there exists a symmetric matrix $\mathbf{Q}$[9]. It can be summarized as for closed-loop system

$$M_{\Re}(\mathbf{A}_{cl}, \mathbf{Q}_{\Re}) < 0, \quad \mathbf{Q}_{\Re} > \tag{23}$$

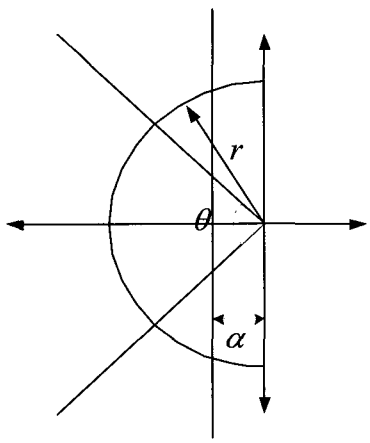

Fig. 3 Pole placement region

For a prescribed closed-loop H_∞ performance $\gamma>0$, our suboptimal mixed H_∞/H_2 problem consists of finding a state-feedback gain $\boldsymbol{K}$ that

- Places the closed-loop poles in LMI stable region $\mathfrak{R}$
- Guarantees the H_∞ performance $\|T_{wz_\infty}\|_\infty < \gamma$
- Minimizes the H_2 performance $\|T_{wz_2}\|_2$ subjected to above two constraints.

But our goal is to minimize the H_2 norm of $\|T_{wz_2}\|_2$ over all state-feedback gains K that enforce H_∞ and pole constraints. From above discussion, this is equivalent to minimizing $trace(\mathbf{Y})$ over all matrices to $\mathbf{Q}_\infty, \mathbf{Q}_2, \mathbf{Q}_\mathfrak{R}, \mathbf{Y}$ and $\mathbf{L}$ satisfying (18), (20), and (23).

To implement multiobjective synthesis, we impose the constraint

$$\mathbf{Q} = \mathbf{Q}_\infty = \mathbf{Q}_2 = \mathbf{Q}_\mathfrak{R} \tag{24}$$

The solution can be sought by substituting (24) into (18), (20), and (23). It can be computed as the global minimum of the following LMI optimization problem. In other words, it make us minimize $trace(\mathbf{Y})$ over $\mathbf{Q}=\mathbf{Q}^T>0$, $\mathbf{Y}=\mathbf{Y}^T$ and $\mathbf{L}$ subject to the LMI constraints.

Assume that (25) is feasible and let $(\mathbf{Q}^*, \mathbf{Y}^*, \mathbf{L}^*, \gamma^*)$ be an optimal solution of this minimization problem. Then the corresponding state-feedback control gain is given by $\mathbf{K}^* = \mathbf{L}^*(\mathbf{Q}^*)^{-1}$ and this gain guarantees H_∞ performance is less than γ^*, places the closed-loop poles in $\mathfrak{R}$, and yields on H_2 performance that does not exceed $\sqrt{trace(\mathbf{Y}^*)}$. From the trade-off curve between H_∞ and H_2 performance, we select best compromise state-feedback control gain $\mathbf{K}$.

$$\begin{bmatrix} \mathbf{AQ}+\mathbf{QA}^T+\mathbf{B}_2\mathbf{L}+\mathbf{L}^T\mathbf{B}_2^T & \mathbf{B}_1 & \mathbf{QC}_\infty^T+\mathbf{L}^T\mathbf{D}_{1\infty}^T \\ \mathbf{B}_1^T & -\gamma^2\mathbf{I} & \mathbf{D}_{11}^T \\ \mathbf{C}_1\mathbf{Q}+\mathbf{D}_{12}\mathbf{L} & \mathbf{D}_{11} & -\mathbf{I} \end{bmatrix} \le 0,\ \mathbf{Q}_\infty>0$$

$$\begin{bmatrix} \mathbf{Y} & \mathbf{C}_2\mathbf{Q}+\mathbf{D}_{22}\mathbf{L} \\ \mathbf{QC}_2^T+\mathbf{LD}_{22}^T & \mathbf{Q} \end{bmatrix} > 0,$$

$$\left[\alpha_{kl}\mathbf{Q}+\beta_{kl}(\mathbf{AQ}+\mathbf{B}_1\mathbf{L})+\beta_{lk}(\mathbf{QA}^T+\mathbf{L}^T\mathbf{B}_2^T)\right]_{1\le k,l\le m} < 0. \tag{25}$$

Model Uncertainty

The notion of uncertain dynamical system is central to robust control theory. The gap between such models and the true physical system is called the model uncertainty. Generally, uncertainties stem from the imperfect knowledge of the system, or the alteration of the physical parameter values due to changes in operation conditions. There are two major classes of uncertainty[8]. In our paper, parameter uncertainty, which originates from imperfect knowledge of the physical parameter values or from variations of these parameters during operation is considered as $\pm 5\,\%$ range of mass and stiffness variations. These uncertainties are represented by uncertain state-space models. Uncertain state-space model is described as[8]

$$\begin{aligned} \mathbf{E}\dot{\mathbf{x}} &= \tilde{\mathbf{A}}\mathbf{x}+\tilde{\mathbf{B}}\mathbf{u} \\ \mathbf{y} &= \mathbf{C}\mathbf{x}+\mathbf{D}\mathbf{u} \end{aligned} \tag{26}$$

where the state-space matrices $\tilde{\mathbf{A}}, \tilde{\mathbf{B}}, \mathbf{C}, \mathbf{D}, \mathbf{E}$ depend on uncertain and/or time-varying parameters or vary in some bounded sets of the spaces of matrices. The dynamic equations of motions often involve uncertain or time-varying coefficients. When the system is linear, it naturally gives rise to parameter-dependent models of the form

$$\begin{aligned} \mathbf{E}(p)\dot{\mathbf{x}} &= \tilde{\mathbf{A}}(p)\mathbf{x}+\tilde{\mathbf{B}}(p)\mathbf{u} \\ \mathbf{y} &= \mathbf{C}(p)\mathbf{x}+\mathbf{D}(p)\mathbf{u} \end{aligned} \tag{27}$$

where $\tilde{\mathbf{A}}(\cdot),\ldots,\mathbf{E}(\cdot)$ are known functions of some

parameter vector $\mathbf{p}=(p_1,\cdots,p_n)$. In our case, $\tilde{\mathbf{A}}(\mathbf{p})$ and $\tilde{\mathbf{E}}(\mathbf{p})$ are defined as below, respectively. And parameter vector is defined as $\mathbf{p}=(m,K_h)$. In other words,

$$\tilde{\mathbf{A}}(\mathbf{p})=\mathbf{A}_0+m\mathbf{A}_m+K_h\mathbf{A}_K$$
$$\mathbf{E}(\mathbf{p})=\mathbf{E}_0+m\mathbf{E}_m+K_h\mathbf{E}_K \tag{28}$$

The parameter uncertainty range can be described as a box in the parameter space. This corresponds to cases where each uncertain or time-varying parameter p_i ranges between two empirically determined extremal values $\underline{p}_i$ and $\overline{p}_i$:

$$p_i\in\left[\underline{p}_i,\overline{p}_i\right] \tag{29}$$

Here we do not consider time-varying parameter, i.e. the rate of variation.

5. Discussion of Results

The geometrical and physical characteristics of the 3-DOF flapped wing system to be used in the present numerical simulations are presented in Table 1. The flutter speed for this model is V_F =139.3 m/s. In order to validate the result present in this paper a comparison is done using the parameters shown in Ref. (10), for which the calculated flutter speed is V_F =271.3 m/s. The critical value of the flutter speed is obtained herein via the solution of both the complex eigenvalue problem and from the subcritical aeroelastic response analysis and an excellent agreement with Ref. (11) is reached.

Table 1 Geometrical parameters of wing model

Parameter	Value
$b=0.3048(\mathrm{m})$	$c=1.0$
$x_{EA}=-0.3$	$m=128.7(\mathrm{kg/m^3})$
$K_\alpha=0.2\times100^2 I_\alpha(\mathrm{kg\cdot m/s^2})$	$I_\alpha=0.25\times26.9(\mathrm{kg/m^2/m})$
$K_\beta=0.2\times300^2 I_\beta(\mathrm{kg\cdot m/s^2})$	$I_\beta=0.25\times0.6727(\mathrm{kg/m^2/m})$
$K_h=0.2\times50^2\mathrm{m(kg\cdot m/s^2)}$	$S_\alpha=0.3\times8.946(\mathrm{kg})$
$\rho=1.225(\mathrm{kg/m^3})$	$S_\beta=0.3\times1.471(\mathrm{kg})$

Fig. 4 shows us trade-off relation between H_∞ performance and H_2 performance. By inspection of this curve, the state-feedback gain obtained for γ =0.03 yields the best compromise between the H_∞ and H_2 objectives.

Singular value plots of nominal and uncertain model are presented in Fig. 5(a) and (b), respectively. We can find three peak values in both nominal and uncertain model. For a square state matrix system, the peak value frequency is referred to the natural frequency of the system. Actually, the plunging, pitching and flapping frequency correspond to the peak value frequency in singular value plots. Fig. 5(a) shows the control performance of the nominal model in frequency domain. Specially, the second peak value of pitching frequency well decreased. Fig. 5(b) shows the control performance of the four uncertain models which have different variations in mass and stiffness. We can see the almost similar controlled response in each uncertain model. Only one uncontrolled uncertain model, possessing the least both mass and stiffness, is plotted in Fig. 5(b). Also that case has the largest peak value in singular value plot. The largest singular value plot refers to the H_∞ norm of the transfer matrix. In both nominal and uncertain model case, the largest singular value is well decreased at pitching frequency.

In case parameter variation exist in the mass

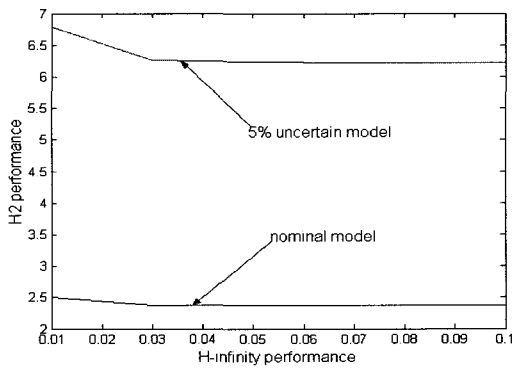

Fig. 4 Trade-off curve between H_∞ and H_2 performance

and stiffness of system, the pitching and plunging displacement exposed to impulse disturbance are presented in Fig. 6 and 7. The upper plot of Fig. 6 shows uncontrolled response for the uncertain model, which is implemented by one set of four extremal values and the same controlled case. Fig. 7 shows the plunging response in comparison with Fig. 6. In both pitching and plunging case, we can make certain that controller works good performance, including nominal case, in spite of the 4 extremal uncertainty values.

We have concerned previous results at subcritical flight speed region. The response to impulse disturbance at flutter speed is shown in Fig. 8. Like our expectation, the large amplitude occurs and response will be unstable with one set of extremal values. Once the controller works, the amplitude decrease in short times remarkably.

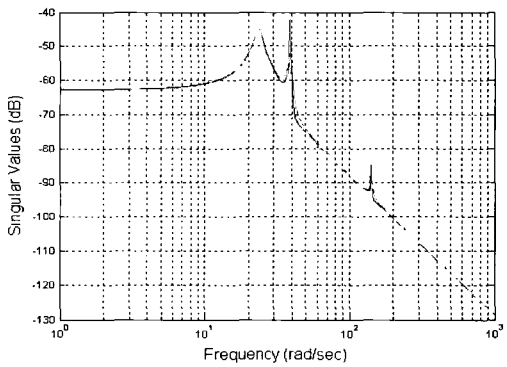

(a) Nominal model

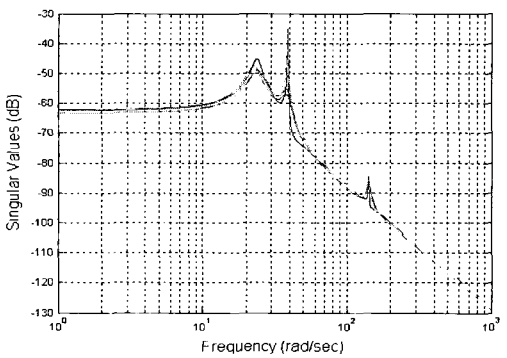

(b) Uncertain model

Fig. 5 (a) and (b) singular value plot of nominal and uncertain model

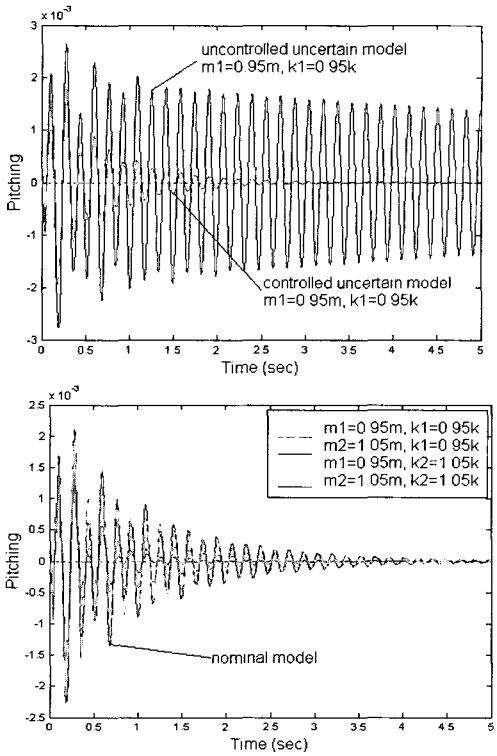

Fig. 6 Pitching displacement with impulse disturbance

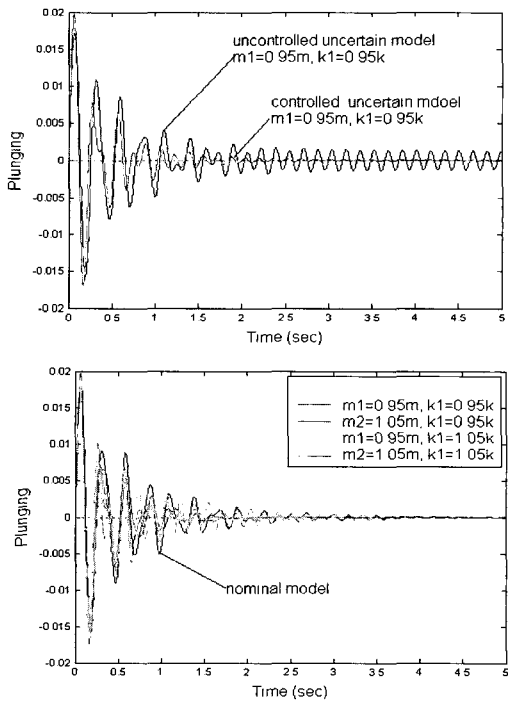

Fig. 7 Plunging displacement with impulse disturbance

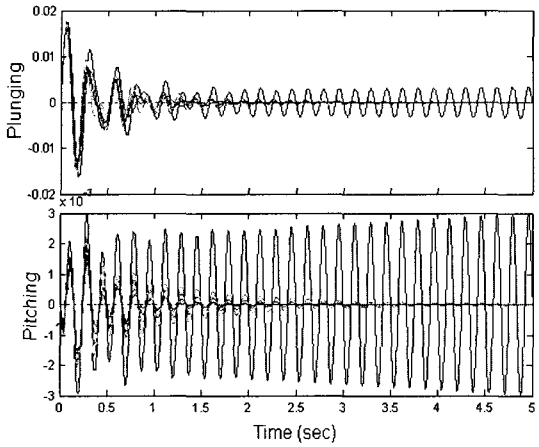

Fig. 8 Robustness to model uncertainty at flutter speed

6. Conclusions

Results related to the aeroelastic response and robust control of 3-DOF flapped wing systems operating in an incompressible flight speed and exposed to impulse disturbance are presented. Also an integrated robust controller design procedure for aeroelastic system with uncertainties due to mass and stiffness variation is addressed. The design procedure involves the solution of a multiobjective optimization problem involving three different constraints on the controller for aeroelastic system. Admittedly with some degree of conservatism, these results offer numerically tractable means of performing multiobjective controller design.

Acknowledgments

Sungsoo Na and In-Joo Jeong acknowledge the support by the Basic Research Program of the Korea Science & Engineering Foundation, Grant No. R01-2002-000-00129-0.

References

(1) Marzocca, P., Librescu, L. and Chiocchia, G., 2001, "Aeroelastic Response of a 2-D Lifting Surfaces to Gust and Arbitrary Explosive Loading Signatures," International Journal of Impact Engineering, Vol. 25, No. 1, pp. 41~65.

(2) Librescu, L. Na, S. Marzocca, P. Chung, C. Kwak, M. "Active Aeroelastic Control of 2-D Wing-flap Systems Operating in an Incompressible Flowfield and Impacted by a Blast Pulse," Journal of Sound and Vibration (in press)

(3) Edwards, J. W., 1977, "Unsteady Aerodynamic Modeling and Active Aeroelastic Control, SUDARR 504, Standford Univ. Also Available as NASA CR-148019.

(4) Dowell, E. H., Crawley, E. F., Curtiss, H. C. Jr., Peters, D. A., Scanlan, R. H. and Sisto, F., 1978, "A Modern Course in Aeroelasticity," Sijthoff and Noordhoff.

(5) Na, S. and Librescu, L., 2000, "Optimal Vibration Control of Thin-walled Anisotropic Cantilevers Exposed to Blast Loading," Journal of Guidance, Control, and Dynamics, Vol. 23, No. 3, pp. 491~500.

(6) Scherer, C., Gahinet, P. and Chilali, M., 1997, "Multiobjective Output-feedback Control via LMI Optimization", IEEE Trans. on Automatic Control, Vol. 42, No. 7, pp. 896~911.

(7) Khargonekar P. P. and Rotea, M. A., 1991, "Mixed H_2/H_∞ control: A Convex Optimization Approach", IEEE Transaction on Automatic Control, Vol. 36, No. 7, pp. 824~837.

(8) Gahinet, P., Nemirovski, A., Laub, A. J. and Chilali, M., 1995, "LMI Control Toolbox", The Math Works Inc.

(9) Chilali, M. and Gahinet, P., 1996, "H_∞ Design with Pole Placement Constraints: An LMI Approach", IEEE Transactions on Automatic Control, Vol. 41, No. 3, pp. 358~367.

(10) Olds, S. D., 1997, "Modeling and LQR Control of a Two-dimensional Airfoil," MS Thesis, Department of Mathematics, Virginia Polytechnic Institute and State University, Blacksburg, VA.

(11) Djayapertapa, L. and Allen, C. B., 2002, "Numerical Simulation of Active Control of Transonic Flutter," Proc. Of the 23rde ICAS Congress, Toronto, 411.1-411.10.